



Preparation of electrocatalysts using a thiol-amine solution processing method

Journal:	<i>Dalton Transactions</i>
Manuscript ID	DT-FRO-02-2018-000442.R1
Article Type:	Frontier
Date Submitted by the Author:	11-Mar-2018
Complete List of Authors:	McCarthy, Carrie; University of Southern California, Chemistry Brutchev, Richard; University of Southern California, Chemistry



Preparation of electrocatalysts using a thiol-amine solution processing method

Received 00th January 20xx,
Accepted 00th January 20xx

DOI: 10.1039/x0xx00000x

www.rsc.org/dalton

Carrie L. McCarthy^a and Richard L. Brutchey^{*a}

Solution processing has emerged as a promising option for the preparation of functional materials with methods that tend to be cheap, less energy intensive, and allow for high throughput and large area deposition. A recently developed method, whereby a binary thiol-amine solvent mixture is used to dissolve bulk oxides, chalcogenides, or elemental materials to yield molecular precursor inks for the deposition of phase pure chalcogenide materials, has recently garnered attention for applications in optoelectronics, thermoelectrics, and electrocatalysis. Presented here is a summary of reports on the application of this “alkahest” method for the deposition of electrocatalytic materials. Ink formulations drawing on the vast library of bulk precursor solutes have already resulted in a large collection of synthesized functional materials, with room still to explore new, or less studied, materials. Additionally, as is seen for the electrocatalysts, engineering of inks and deposition procedures can lead to higher performance through optimized morphology and form factors.

Introduction

In the face of anthropogenic climate change we must begin to think and act based on a systems approach rather than addressing problems as discrete events. Regarding the design of products, we should not only design for sustainability in the direct use of a product, but also for low-impact fabrication as well as possible reuse, upcycling, or recycling. Specifically, for the design of functional inorganic materials, such as catalysts and semiconductors, we must consider the various impacts, beyond functionality, of choosing specific elements and sources to incorporate into materials. For example, while noble metals such as platinum and palladium are excellent catalysts for a wide range of very important reactions, including the hydrogen evolution reaction (HER), they are also rare in the crust of the Earth.^{1,2} Deploying them at scale, even for sustainable technologies such as hydrogen production for clean fuel, would lead to more instability in a system (already dominated by the demands of the auto, jewelry, chemical, electrical, and medical industries) dependent on scarce resources, not to mention the high capital and social costs of mining and refining the metals relative to the quantities recovered.^{2–4} In considering these and other big-picture issues, researchers have developed alternative catalyst materials containing more Earth-abundant elements such as molybdenum, nickel, cobalt, and iron.^{5,6} Earth-abundant

materials are also being developed for application as semiconductor absorbers for photovoltaics (PV), battery electrode materials, and thermoelectrics.^{7–12}

A second aspect of a systems approach to functional materials is the design of versatile, low-impact, high-throughput fabrication processes. Currently, the industry standards for fabricating functional inorganic materials are energetically and financially burdensome, requiring capital-intensive hardware and energy-intensive deposition processes. As such, there is room for improvements toward more cost- and energy-effective manufacturing methods. In this Feature Article, we highlight a solution processing method for the deposition of a wide range of functional inorganic materials. This method is an example for which a systems approach has been used to couple Earth-abundant compositions with sustainable manufacturing and the possibility for reuse or recycling.

There are a handful of solution processing methods for the synthesis and deposition of inorganic functional materials, including chemical bath deposition, colloiddally stable nanoparticle inks, sol-gel solutions, and molecular precursor inks.¹³ Colloidal nanoparticle inks and molecular precursor inks are two of the most promising approaches when considering cost and energy requirements as they lend themselves to established techniques such as ink-jet printing.^{14,15} However, in most cases, colloidal nanoparticle inks require separate steps for nanoparticle synthesis, purification, and solution processing, often including multiple washing steps or ligand exchanges. Molecular precursor inks prepared from bulk materials, on the other hand, can be prepared in a single dissolution step followed by direct deposition onto a suitable

^a Department of Chemistry, University of Southern California, Los Angeles, California 90089, United States
E-mail: brutchey@usc.edu
See DOI: 10.1039/x0xx00000x

substrate. Furthermore, the composition of molecular inks can be easily tuned by simply changing the formulation of the ink, and the very nature of such precursor inks facilitates thorough mixing on the molecular level to yield more compositionally homogeneous films.¹⁵ Although direct dissolution of inorganic precursors to give molecular inks is an ideal method for solution processing of functional thin films, most bulk inorganic materials are completely insoluble in common solvents, and until recently, there has been little progress in developing solvent systems that are capable of this.

Alkahest Method

In 2013, our group developed a novel binary solvent system comprised of ethylenediamine (en) and a short chain thiol that is capable of dissolving several bulk inorganic materials. We first showed that nine V_2VI_3 ($V = \text{As, Sb, Bi}$; $VI = \text{S, Se, Te}$) semiconductors can be dissolved in a 1:4 (vol/vol) mixture of ethanedithiol (EDT) and en to give inks from which the sulfide and selenide materials could be recovered upon mild annealing (270–350 °C) in a nitrogen atmosphere.¹⁶ The dissolution of these materials can be done under ambient conditions, at room temperature, and in a matter of minutes. Such benign ink formulation conditions, combined with the ability to recover phase-pure thin films, lead us to further develop this method. In the following year, we showed that the bulk elemental chalcogens (i.e., grey Se and Te) are readily soluble under ambient conditions in thiol-amine solvent systems, and while phase-pure Se can be recovered from its corresponding ink upon low temperature annealing (250 °C), phase pure crystalline Te can be recovered by simply drying the ink at room temperature (in the case of an ethanedithiol/en ink).¹⁷ Additionally, Sb-Se and Sn-Te inks were prepared by dissolving the corresponding elemental precursors at 60 °C, while elemental Sb and Sn showed negligible solubility in the solvent system in the absence of chalcogen. Phase-pure Sb_2Se_3 and SnTe were recovered by annealing their respective precursor inks to 250 °C. To demonstrate that materials outside of the V_2VI_3 family were also accessible using the alkahest method, we used bulk SnS as a precursor to prepare high-quality SnS thin films showing promising photovoltaic properties.¹⁸ Inspired by the work done on metal chalcogenide complex ligands for nanoparticles, we studied the solutes resulting from the dissolution Sb_2S_3 in an alkahest ink, revealing their molecular nature and capability to displace long chain native ligands on the surface of nanoparticles to give higher photocurrent density in nanoparticle thin films.¹⁹

We next sought to expand the library of precursors available for ink formulation, and in turn shine light on the vast assortment of possible material compositions accessible through the alkahest method. In 2015, we reported on the solubility of ten bulk oxides (Cu_2O , ZnO , GeO_2 , As_2O_3 , Ag_2O , CdO , SnO , Sb_2O_3 , PbO , and Bi_2O_3) in alkahest solvent systems, and the recovery of corresponding sulfides (ZnS , Ag_2S , CdS ,

SnS , Sb_2S_3 , and PbS) upon direct annealing of the inks. When elemental Se or Te were added to the inks, selenides (Cu_2Se , ZnSe , CdSe , Ag_2Se and Sb_2Se_3) and tellurides (Ag_2Te , and PbTe) were recovered.²⁰ In addition, we showed how simply tuning the Se content in a Sb_2O_3 -Se ink results in compositionally controlled $\text{Sb}_2\text{Se}_{3-x}\text{S}_x$ alloys with tunable band gaps from 1.2–1.6 eV, ideal for photovoltaic applications. With such a broad toolbox of precursors, including bulk chalcogenides, oxides, and elemental materials, we and other researchers aimed for more complex functional materials. Several groups recognized the value in tailoring the alkahest method toward promising photovoltaic (PV) materials such as $\text{CuIn}_x\text{Ga}_{(1-x)}\text{Se}_2$ (CIGS) and $\text{Cu}_2\text{ZnSnS}_4$ (CZTS), ultimately preparing PV devices with up to 12.2% and 8.0% power conversion efficiencies, respectively.^{21–23} As an Earth-abundant alternative to CIGS, we prepared high quality thin films of CuSbS_2 with a near-ideal band gap (1.6 eV) and promising electronic properties for use as a PV absorber layer.²⁴ More recently, we reported on the first example of solution processed $\text{Cu}_2\text{BaSnS}_4$, a material belonging to a group of CIGS/CZTS alternative chalcogenide semiconductors that have garnered recent interest for PV applications.²⁵

In addition to the need for more Earth-abundant and highly active alternatives to noble metal-based catalysts for HER, the oxygen evolution reaction (OER), and other important catalytic processes such as reduction of triiodide in the $3\text{I}^-/\text{I}_3^-$ redox couple for dye-sensitized solar cells (DSSCs) and reduction of polysulfides in the $\text{S}^{2-}/\text{S}_n^{2-}$ redox couple for quantum dot-sensitized solar cells (QDSCs), is the need for sustainable production of these electrocatalytic materials. Recent advances in the area have provided several promising candidates for replacing expensive catalysts, and many of these are transition metal dichalcogenides (e.g., NiSe_2 , CoSe_2 , MoS_2 , FeS_2 , CoS_2 , NiS_2).^{26–29} Although the majority of application-oriented work using the alkahest method focuses on thin films for PV, there is a growing number of demonstrations of materials prepared as electrocatalysts.^{30–34} The remainder of this article will explore the work that has been done using the alkahest method to prepare electrocatalysts. In analyzing the electrochemical performance of the materials, metrics of specific importance regarding the kinetics and efficiency of heterogeneous electrocatalysis include Tafel slope, exchange current density (i_0 ; i.e., current density when $\eta = 0$), charge transfer resistance (R_{ct}), and Faradaic efficiency.³⁵ Specifically useful for HER and OER electrocatalysts is the benchmark value of overpotential required to produce a current density of 10 mA cm^{-2} ($\eta_{10\text{mA cm}^{-2}}$).³⁶ Fast kinetics and high efficiencies allow for lower catalyst loadings, which at scale translates into more sustainable extraction and utilization of raw materials, and overall cost savings.

Electrocatalysts



Fig. 1 Images of the alkahest inks formulated using the labelled bulk precursors for the deposition of electrocatalysts. (a-c) Adapted from F. Liu, J. Zhu, L. Hu, B. Zhang, J. Yao, M. K. Nazeeruddin, M. Grätzel and S. Dai, *J. Mater. Chem. A*, 2015, **3**, 6315–6323 with permission of The Royal Society of Chemistry. (d) Adapted from X. Zhao, J. Jiang, Z. Xue, C. Yan and T. Mu, *Chem. Commun.*, 2017, **53**, 9418–9421 with permission of The Royal Society of Chemistry. (e) Adapted with permission from C. L. McCarthy, C. A. Downes, E. C. Schueller, K. Abuyen and R. L. Brutchey, *ACS Energy Lett.*, 2016, **1**, 607–611. Copyright 2016 American Chemical Society. (f) Adapted with permission from F. Liu, J. Zhu, Y. Li, J. Wei, M. Lv, Y. Xu, L. Zhou, L. Hu and S. Dai, *J. Power Sources*, **292**, 7–14. Copyright 2015 Elsevier. (g) Adapted with permission from C. L. McCarthy, C. A. Downes and R. L. Brutchey, *Inorg. Chem.*, 2017, **56**, 10143–10146. Copyright 2017 American Chemical Society.

The earliest demonstration of alkahest-synthesized materials working as electrocatalysts was reported by Liu et al. in 2015 wherein they prepared counter electrodes for DSSCs (FeSe₂) and QDSCs (CuSe and Cu_{1.8}S).³⁰ Dissolving tetragonal FeSe, monoclinic Cu_{1.9}S, and monoclinic Cu₂Se precursors in a 10:1 vol/vol mixture of EDT/en under ambient conditions resulted in inks (Fig. 1 a-c) that, upon annealing to 330 °C, yielded phase-pure orthorhombic FeSe₂, hexagonal Cu_{1.8}S, and hexagonal CuSe, respectively. It is of note that both phase and stoichiometry change in each case, and while the authors offer some possible rationalizations (e.g., oxidation of the ink or partial volatilization of the metals), they were unable to prove exactly why this occurs. Uniform electrode films (ca. 25 μm

thick) of each material were deposited by drop casting the inks onto FTO/glass substrates. Scanning electron microscopy (SEM) micrographs (Fig. 2a-c) revealed clusters of 200–300 nm discs in the case of FeSe₂ and Cu_{1.8}S, while the CuSe took the form of clusters of ~100 nm sheets. All three materials had high specific surface areas; i.e., FeSe₂ = 22.5 m² g⁻¹, CuSe = 29.3 m² g⁻¹, and Cu_{1.8}S = 24.0 m² g⁻¹. To assess the suitability of the FeSe₂ as a counter electrode for DSSCs, its electrochemical activity was compared to that of Pt in an iodide/triiodide electrolyte. Cyclic voltammetry (CV) experiments (Fig. 3a) revealed strong electrochemical stability of the FeSe₂ over 10 CV cycles and higher peak currents with smaller peak-to-peak separation when compared to the Pt electrode, thus indicating higher catalytic activity toward the reduction of triiodide. Additionally, electrochemical impedance spectroscopy (EIS) on symmetrical thin film cells showed that in comparison to Pt, FeSe₂ had a lower R_{ct} and a larger diffusion coefficient for the iodide species, both pointing to faster kinetics for the FeSe₂ electrode. The superior electrocatalytic activity of FeSe₂ was further confirmed by polarization curves obtained for the symmetrical cells, which indicated higher *I*₀ and higher limiting current for FeSe₂ as compared to Pt. In agreement with the preliminary electrochemical findings, full DSSCs with FeSe₂ cathodes (9.10% avg. PCE) outperformed those with a Pt cathode (8.42% avg. PCE). CuSe and Cu_{1.8}S electrodes were also studied for their catalytic activity, though as prospective counter electrodes for QDSCs, which use a polysulfide-based electrolyte. Both CuSe and Cu_{1.8}S proved to be electrochemically robust with reproducible CV cycling in the polysulfide electrolyte; the same experiment with a Pt electrode resulted in rapid decay of current density upon

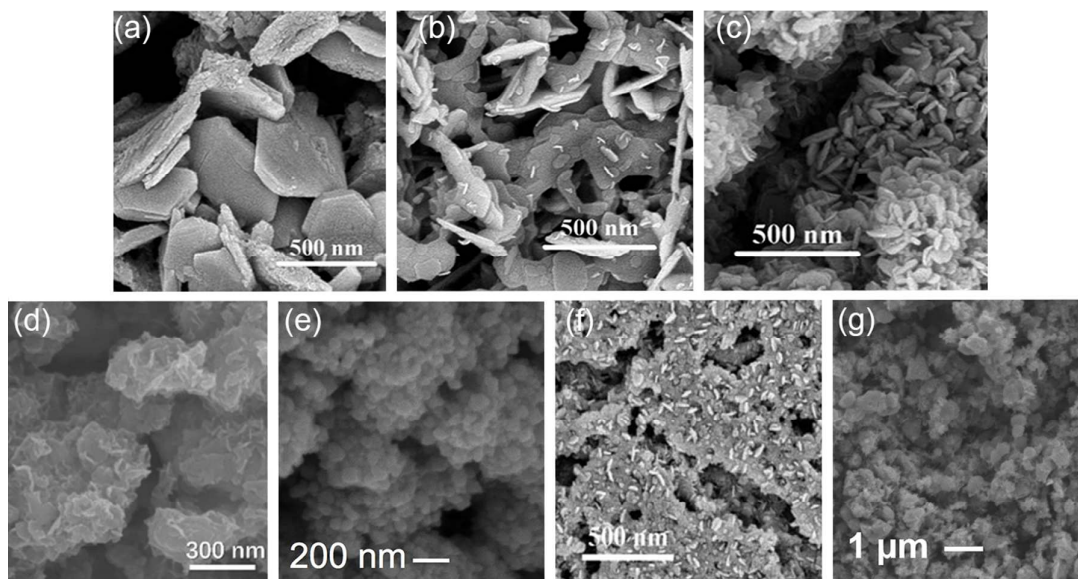


Fig. 2 SEM micrographs showing the nano- and microstructured morphology of (a) FeSe₂, (b) Cu_{1.8}S, (c) CuSe, (d) CoS_x, (e) CoSe₂, (f) Cu₂SnSe₃, and (g) NiSe₂ electrocatalyst materials prepared using alkahest inks. (a-c) Adapted from F. Liu, J. Zhu, L. Hu, B. Zhang, J. Yao, M. K. Nazeeruddin, M. Grätzel and S. Dai, *J. Mater. Chem. A*, 2015, **3**, 6315–6323 with permission of The Royal Society of Chemistry. (d) Adapted from X. Zhao, J. Jiang, Z. Xue, C. Yan and T. Mu, *Chem. Commun.*, 2017, **53**, 9418–9421 with permission of The Royal Society of Chemistry. (e) Adapted with permission from C. L. McCarthy, C. A. Downes, E. C. Schueller, K. Abuyen and R. L. Brutchey, *ACS Energy Lett.*, 2016, **1**, 607–611. Copyright 2016 American Chemical Society. (f) Adapted with permission from F. Liu, J. Zhu, Y. Li, J. Wei, M. Lv, Y. Xu, L. Zhou, L. Hu and S. Dai, *J. Power Sources*, **292**, 7–14. Copyright 2015 Elsevier. (g) Adapted with permission from C. L. McCarthy, C. A. Downes and R. L. Brutchey, *Inorg. Chem.*, 2017, **56**, 10143–10146. Copyright 2017 American Chemical Society.

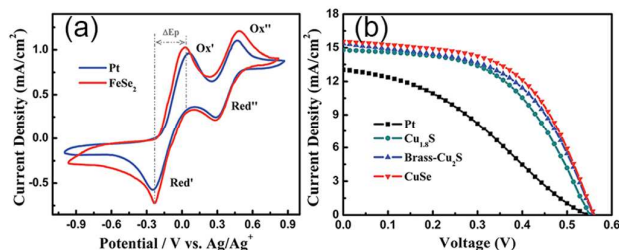


Fig. 3 (a) CV scans of an FeSe₂ electrode compared to that of a Pt electrode in iodide/triiodide electrolyte and (b) QDSC I-V curves for devices employing various counter electrodes as compared to Pt. Adapted from F. Liu, J. Zhu, L. Hu, B. Zhang, J. Yao, M. K. Nazeeruddin, M. Grätzel and S. Dai, *J. Mater. Chem. A*, 2015, **3**, 6315–6323 with permission of The Royal Society of Chemistry.

cycling due to poisoning of the Pt surface. The CuSe material was by far the best catalyst for polysulfide reduction, generating up to 10 times the current density of the Pt electrode and having the highest I_0 and lowest R_{ct} ($0.7 \Omega \text{ cm}^2$); Cu_{1.8}S followed a close second with $R_{ct} = 0.9 \Omega \text{ cm}^2$ while Pt had the lowest I_0 and a very large $R_{ct} = 420.0 \Omega \text{ cm}^2$ (high performing counter electrodes for QDSCs of this type are expected to have an $R_{ct} < 1 \Omega \text{ cm}^2$). QDSCs made using the CuSe, Cu_{1.8}S, Pt, and Cu₂S/brass (a commonly used counter electrode for QDSCs) as counter electrodes gave the expected relative performance as predicted by the electrochemical studies—giving PCEs of 4.89%, 4.31%, 2.48%, and 4.60%, respectively (I - V curves for the QDSCs are plotted in Fig. 3b). Reproducibility and durability of all three chalcogenide electrodes was demonstrated by finding similar results on different batches of materials and by reusing the electrodes.

Using a unique approach, Zhao et al. prepared amorphous nanostructured CoS_x as an OER electrocatalyst by adapting their method for precipitating materials out of ionic liquids, using pressurized CO₂ as an antisolvent.^{31,37,38} Co-dissolution of elemental cobalt and sulfur in an EDT/*n*-butylamine mixture under ambient conditions was accomplished in less than 1 h to yield an olive brown ink after filtering (Fig. 1d). It was found that elemental Co was not soluble in the solvent mixture on its own, only in the presence of sulfur. Precipitation of amorphous CoS_x was achieved by pressurizing an autoclave containing the ink to 6 MPa with CO₂ for 3 h (the authors were also able to synthesize FeS_x, NiS_x, and CoS_xSe_y using this precipitation method). The intensity of the signal observed in the UV-vis absorption spectrum of the ink corresponding to

Co-S species decreased as the time under compressed CO₂ increased, consistent with the loss of Co-S species in solution upon precipitation. Powder X-ray diffraction (XRD) data showing no obvious diffraction peaks suggested that the recovered material was amorphous, and SEM micrographs (Fig. 2d) revealed a hierarchical structure of assembled 200–300 nm-wide nanosheets (BET specific surface area = $24.2 \text{ m}^2 \text{ g}^{-1}$; pore volume $0.0736 \text{ cm}^3 \text{ g}^{-1}$). Energy dispersive X-ray spectroscopy (EDX) showed that the material was comprised of only Co and S in a ratio of 1:1.06; inductively coupled plasma optical emission spectroscopy (ICP-OES) elemental analysis gave a similar ratio of 1:1.10. X-ray photoelectron spectroscopy (XPS) analysis showed oxidation of the CoS_x surface with a Co²⁺/Co³⁺ ratio of ~1.8, both S²⁻ and S⁶⁺ species, and multiple peaks in the O 1s region. In addition to Co-S signals, Raman spectroscopy confirmed the presence of Co-OH bands. To study the effect of electrode support, electrochemical measurements of the CoS_x were conducted by depositing the material on glassy carbon, single crystalline Au(111), and gold-plated Ni-foam electrodes. In 1.0 M KOH, $\eta_{10 \text{ mA cm}^{-2}}$ was reached at overpotentials of 302 mV, 386 mV, and 271 mV for the glassy carbon, Au(111), and gold-plated Ni-foam electrodes, respectively (compared to state-of-the-art IrO₂ with $\eta_{10 \text{ mA cm}^{-2}} = 340 \text{ mV}$). A similar trend was observed for the Tafel slopes; that is, 64.8 mV dec^{-1} on glassy carbon, 84.2 mV dec^{-1} on Au(111), and 48.8 mV dec^{-1} on gold-plated Ni-foam. From these data, it was concluded that: (1) choice of electrode substrate is quite important, with the high surface area gold-plated Ni-foam giving the best OER performance, and (2) the CoS_x prepared in this work performed better than the state-of-the-art Co-based OER catalysts at the time (e.g., $\eta_{10 \text{ mA cm}^{-2}} = 290\text{--}430 \text{ mV}$ and Tafel slopes = $47\text{--}85 \text{ mV dec}^{-1}$). Continuous electrochemical stability testing was done on the gold-plated Ni-foam sample by holding the electrode at a constant current of 30 mA cm^{-2} for 300 h, and revealing no observable decrease in potential with a Faradaic efficiency of ca. 99%. Annealing to 400 °C and 800 °C resulted in crystallization of the amorphous CoS_x, a decrease in the specific surface area, and decreased OER performance. In addition to the smaller surface area, the authors attribute the decreased activity to the fact that amorphous cobalt sulfide materials have been shown to be more active than their highly crystalline counterparts.^{39,40}

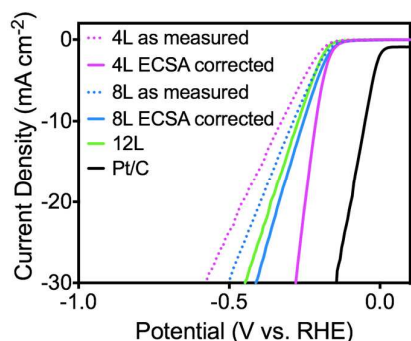


Fig. 4 Polarization curves in acidic solution for various loadings of CoSe₂ on HOPG substrates. As-measured data (solid traces) and data corrected for experimentally determined ECSA (dotted traces) are shown. Reprinted with permission from C. L. McCarthy, C. A. Downes, E. C. Schueller, K. Abuyen and R. L. Brutchey, *ACS Energy Lett.*, 2016, 1, 607–611. Copyright 2016 American Chemical Society.

We next demonstrated that the alkahest method could be used to prepare HER electrocatalysts.³² Co-dissolution of Co(OH)₂ and elemental Se in a mercaptoethanol/en mixture over the course of 20 min gives an optically clear green precursor ink after filtration (Fig. 1e). The ink has an organic decomposition end point of ca. 350 °C by thermogravimetric analysis (TGA), which is confirmed by the loss of ν(O-H), ν(N-H), and ν(C-H) stretches in the FT-IR spectrum. When annealed to 350 °C, the ink yields phase-pure, orthorhombic marcasite-type CoSe₂, as confirmed by XRD (with the same material also being recovered when EDT or ethanethiol are used as the thiol component in the ink) and verified by lattice fringes observed by high resolution transmission electron microscopy (HR-TEM). XPS corroborated the XRD findings of marcasite-type CoSe₂ by revealing a single Co species in the 2+ oxidation state, and similarly, a single Se species identified as Se₂²⁻. The bulk composition of the material was confirmed to be CoSe_{2.2} by both ICP-OES and SEM-EDX. SEM micrographs (Fig. 2e) of the recovered material showed that it is comprised of nanostructured grains 75–100 nm in size; such a morphology yields higher surface areas and is beneficial for high catalytic activity. The filtered precursor ink was easily deposited onto highly ordered pyrolytic graphite (HOPG) substrates in multiple layers by spin coating followed immediately by annealing at 350 °C between coats. Deposition of 4, 8, and 12 layers of ink gave thin films with thicknesses of 151, 258, and 391 nm, respectively. In 0.5 M H₂SO₄, the 4-, 8-, and 12-layered samples had the same onset potential (117 mV), similarly low Tafel slopes (55–62 mV dec⁻¹), and exhibited 99% Faradaic efficiency. However, the samples had decreasing η_{10 mA cm⁻²} values of 327 mV, 287 mV, 272 mV for 4, 8, and 12 layers, respectively. The 12-layered CoSe₂ electrode performed on par with the higher end of the range of reported η_{10 mA cm⁻²} values for HER using Earth abundant electrocatalysts (i.e., 50 – 275 mV).⁴¹ Double layer capacitance measurements were used to calculate the electrochemically active surface area (ECSA) for each of the three samples, which revealed an increase in ECSA with increased CoSe₂ loading. When the polarization curves were normalized with respect to ECSA (Fig. 4), it was revealed that

the 4-layered sample actually had the lowest relative η_{10 mA cm⁻²}, followed by the 8- and 12-layered samples. This is explained by a mass transport-dominated process at high overpotentials—while ECSA is measured using CV at low overpotentials with non-Faradaic current (by which the 12-layered sample was characterized as having the largest available area for electrochemical processes), the actual surface area during high overpotential-driven HER is limited by the mass transport of molecules to the inner-most surfaces of the catalyst. Therefore, we concluded that in order to achieve the most efficient surface utilization of the CoSe₂ catalyst, thinner layers are preferred. A stability test on the 12-layered sample, in which the overpotential required to produce a current density of 20 mA cm⁻² (η_{20 mA cm⁻²}) was measured, revealed no change in η_{20 mA cm⁻²} after 8 h in 0.5 M H₂SO₄ (as protons were consumed in the HER reaction, the solution pH increased, resulting in higher η_{20 mA cm⁻²} values; after 5 h the electrolyte solution was replaced with fresh 0.5 M H₂SO₄ returning η_{20 mA cm⁻²} to the initial value). In addition, the preservation of curve shape in polarization curves measured for the sample in 1 h increments indicated no change in the electrocatalytic process over the course of 8 h. By easily tuning the catalyst layer thickness via solution deposition, we showed how such an electrocatalytic system might be optimized to give maximum catalyst utilization.

Zhu, Dai, and co-workers followed their initial work on QDSC and DSSC counter electrodes (vide supra) with a similar report on alkahest-processed Cu₂SnSe₃ as a counter electrode for QDSCs using a polysulfide electrolyte.³³ The precursor ink was prepared using Cu₂Se and SnSe as bulk precursors dissolved in a 1:10 vol/vol mixture of EDT/en under nitrogen at 75 °C for 24 h (Fig. 1f). After annealing the ink to 370 °C, phase-pure monoclinic Cu₂SnSe₃ was recovered, as verified by XRD and Raman spectroscopy, with no sign of SnSe_x or Cu_xSe phases. Of note, the elemental composition used in the ink formulation was a Cu:Sn:Se ratio of 3.12:2:2.56, while the stoichiometry of the recovered product is 2:1:3. Such changes in chemical composition from ink formulation to recovered material have been observed before for this type of solution processing, and the authors postulate that this discrepancy is accounted for by the selective volatilization of metallic elements during the annealing process.^{22,30} Thin films were deposited by spin coating the ink onto FTO/glass substrates followed by annealing. SEM was used to study the morphology of the films (Figs. 2f and 5), revealing homogeneous and dense

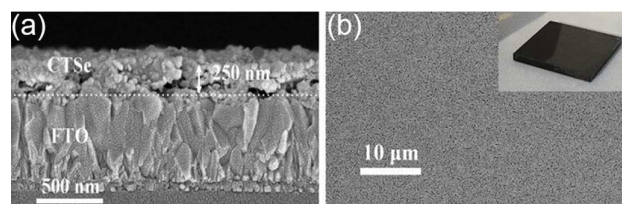


Fig. 5 (a) Cross-section and (b) top-view SEM micrographs of a uniform Cu₂SnSe₃ thin film on an FTO substrate. A photograph of the spin-coated electrode is shown in the upper right corner of (b). Adapted with permission from F. Liu, J. Zhu, Y. Li, J. Wei, M. Lv, Y. Xu, L. Zhou, L. Hu and S. Dai, *J. Power Sources*, 2015, 292, 7–14. Copyright 2015 Elsevier.

polycrystalline (ca. 20-60 nm crystallites) films with a thickness of ca. 250 nm. The specific surface area ($38.15 \text{ m}^2 \text{ g}^{-1}$) and surface roughness (28.9 nm) were also analyzed. The electrocatalytic activity of the Cu_2SnSe_3 films was first studied using a symmetric cell made using two $\text{Cu}_2\text{SnSe}_3/\text{FTO}/\text{glass}$ (or Pt, for comparison) electrodes with polysulfide electrolyte sandwiched in between. From EIS, R_{ct} values of $0.3 \Omega \text{ cm}^2$ and $427.1 \Omega \text{ cm}^2$ were determined for Cu_2SnSe_3 and Pt, respectively. While the direct band gap of the recovered Cu_2SnSe_3 was determined as $E_{\text{g,dir.}} = 1.25 \text{ eV}$ by UV-vis absorbance spectroscopy, indicating possible photocatalytic activity, the R_{ct} value was unchanged by illumination of the cell with 100 mW cm^{-2} light. Polarization curves obtained from symmetrical cells revealed a higher I_0 and limiting current for the Cu_2SnSe_3 compared to Pt, indicating higher catalytic activity and faster diffusion of S_n^{2-} for Cu_2SnSe_3 . CV measurements on both types of electrodes showed higher reduction current density at any given reduction potential in the case of Cu_2SnSe_3 compared to Pt, indicating a faster rate of reduction of S_n^{2-} to S^{2-} . Additionally, after 10 cycles, the Cu_2SnSe_3 retained its high current density while the current density of the Pt electrode dropped to nearly half its original value (as a result of surface chemisorption of sulfur species). Full QDSCs prepared using the Cu_2SnSe_3 , Pt, and brass- Cu_2S electrodes gave photocurrent-voltage curves revealing that the Cu_2SnSe_3 outperformed both the Pt-based and brass- Cu_2S cells on all metrics (i.e., V_{OC} , J_{SC} , FF, PCE), with average PCEs of 4.93%, 2.27%, and 4.64%, respectively. The low R_{ct} value of the Cu_2SnSe_3 electrodes, and thus higher catalytic activity due to faster electron transfer from the electrode to the S_n^{2-} species, was found to be the major contributor to the higher QDSC performance. Additionally, compared to the Pt electrode, the Cu_2SnSe_3 electrode produced a higher reflectance at all wavelengths from 400 – 800 nm as measured by UV-vis spectroscopy, which reduces loss of incident light and increases photon absorption. Cu_2SnSe_3 -based QDSCs exhibited higher stability in a 12 h light soaking stability test when compared to the brass- Cu_2S devices.

Following our initial report on CoSe_2 , we reported on the preparation of cubic pyrite-type NiSe_2 thin films for HER using bulk elemental Ni and Se as precursors in a mercaptoethanol/enk ink (Fig. 1g).³⁴ The ink was prepared by dissolving the bulk precursors in the binary solvent mixture over 48 h followed by filtration, to yield a rusty-orange-colored ink. The endpoint of decomposition for the ink was observed by TGA as ca. $350 \text{ }^\circ\text{C}$, and upon annealing the ink to this temperature, XRD analysis confirmed that phase-pure pyrite-type NiSe_2 was recovered. FT-IR analysis also showed loss of all organics by $350 \text{ }^\circ\text{C}$. XPS was used to study the surface composition of the material and revealed a single species for both Ni (Ni^{2+}) and Se (Se_2^{2-}) as expected for pyrite-type NiSe_2 . Additionally, there was no sign of nickel oxide (i.e., NiO) or oxidized selenium species (i.e., SeO_x). SEM-EDX verified a near-perfect stoichiometry of $\text{NiSe}_{2.06}$ with ca. 1 at% S, remaining from mercaptoethanol decomposition. A nanostructured morphology was observed by SEM (Fig. 2g) with grains on the order of 200-700 nm, indicating promise for high catalytic

surface area. Electrochemical measurements were conducted in a solution of 0.5 M H_2SO_4 for samples prepared by spin coating 4, 6, and 8 layers of the precursor ink on HOPG substrates (and annealing to $350 \text{ }^\circ\text{C}$ between coats). Similar to the CoSe_2 study (vida supra), the various loadings of NiSe_2 had nearly identical onset potentials, Tafel slopes, and exchange current densities (i.e., 130 mV, $35\text{-}40 \text{ mV dec}^{-1}$, and $10^{-6} \text{ mA cm}^{-2}$), as well as 100% Faradaic efficiency. These performance metrics are all similar to previous literature examples of NiSe_2 electrodes under similar conditions. The $\eta_{10 \text{ mA cm}^{-2}}$ values decrease as NiSe_2 loading increases (similar to the CoSe_2 study): 328 mV, 277 mV, and 269 mV for 4, 6, and 8 layers, respectively. Unlike the CoSe_2 electrodes, when the polarization curves for the NiSe_2 films were corrected for ECSA, a similar $\eta_{10 \text{ mA cm}^{-2}}$ value was found for all samples, indicating that the surface utilization of the NiSe_2 films did not decrease with catalyst loading under the given conditions. Nyquist plots generated from EIS analysis showed the general trend of decreasing R_{ct} with increased NiSe_2 loading and with increased applied potential, as expected for increasing the amount of active sites and increasing the driving force, respectively. Diffusion limitations at much higher overpotentials (i.e., 450 mV) were indicated by a decrease in the relative difference in R_{ct} values for the different loadings as higher overpotentials were applied.

Conclusion

As demonstrated by these recent reports on electrocatalysts prepared using inks derived from bulk material dissolution in a thiol-amine solvent mixture, the alkalest solution processing method shows promise for the development of electrocatalytic chalcogenide materials. For example, OER and HER electrocatalysts described herein perform on par with other chalcogenide materials, prepared by more conventional methods (e.g., $\eta_{10 \text{ mA cm}^{-2}} = 90\text{-}260 \text{ mV}$ for HER and $200\text{-}360 \text{ mV}$ for OER).^{6,42} Furthermore, in light of recent achievement of impressive performances using unique nanostructuring of chalcogenide electrocatalysts, e.g., HER $\eta_{10 \text{ mA cm}^{-2}} = 57 \text{ mV}$ for NiSe_2 , material engineering (e.g., deposition method, film thickness, form factor) paired with the alkalest system holds promise to yield superior results, even for the materials already reported.²⁶

This method is also a facile way to prepare and study the electrocatalytic properties of previously unstudied materials as it is very easy to tune ink formulation by adjusting which precursors are used and in what quantities. Additionally, it has been observed in some cases that, all else being held the same, changing the thiol or amine in the solvent mixture can lead to different material phases upon annealing.^{20,43} Paralleling the efforts toward preparing high performance functional materials, future work in this area must also focus on the mechanisms at play in the dissolution of precursors and recovery of chalcogenide materials. This will ultimately lead to more precise compositional and phase control over the recovered materials. In this way we can aim for precision in

accessing ideal materials for various applications while maintaining low impact production.

Conflicts of interest

There are no conflicts to declare.

Acknowledgements

This work was supported by the National Science Foundation (NSF) under grant DMR-1506189. C.L.M. thanks the NSF for a graduate research fellowship.

References

- J. R. McKone, S. C. Marinescu, B. S. Brunschwig, J. R. Winkler and H. B. Gray, *Chem. Sci.*, 2014, **5**, 865–878.
- M. L. Zientek, P. J. Loferski, H. L. Parks, R. F. Schulte and R. R. I. Seal, *Platinum-group elements*, Reston, VA, 2017.
- PGM Market Report May 2017*, Johnson Matthey Precious Metals Management, 2017.
- G. M. Mudd, S. M. Jowitt and T. T. Werner, *Sci. Total Environ.*, 2018, **622–623**, 614–625.
- F. M. Sapountzi, J. M. Gracia, C. J. Weststrate, H. O. A. Fredriksson and J. W. Niemantsverdriet, *Prog. Energy Combust. Sci.*, 2017, **58**, 1–35.
- I. Roger, M. A. Shipman and M. D. Symes, *Nat. Rev. Chem.*, 2017, **1**, 3.
- R. Haight, T. Gershon, O. Gunawan, P. Antunez, D. Bishop, Y. S. Lee, T. Gokmen, K. Sardashti, E. Chagarov and A. Kummel, *Semicond. Sci. Technol.*, 2017, **32**, 033004.
- C. P. Grey and J. M. Tarascon, *Nat. Mater.*, 2017, **16**, 45–56.
- D. Larcher and J. M. Tarascon, *Nat. Chem.*, 2015, **7**, 19–29.
- R. D. Schmidt, E. D. Case, L. Zhao and M. G. Kanatzidis, *J. Mater. Sci.*, 2015, **50**, 1770–1782.
- J. Yang, Q. Yuan, H. Deng, S. Wei and B. I. Yakobson, *J. Phys. Chem. C*, 2017, **121**, 123–128.
- S. Chu, Y. Cui and N. Liu, *Nat. Mater.*, 2017, **16**, 16–22.
- D. B. Mitzi, *Solution Processing of Inorganic Materials*, John Wiley & Sons, Hoboken, New Jersey, 2008.
- S. Magdassi and A. Kamyshny, *Nanomaterials for 2D and 3D Printing*, John Wiley & Sons, Weinheim, Germany, 2017.
- D. B. Mitzi, *Adv. Mater.*, 2009, **21**, 3141–3158.
- D. H. Webber and R. L. Brutchey, *J. Am. Chem. Soc.*, 2013, **135**, 15722–15725.
- D. H. Webber, J. J. Buckley, P. D. Antunez and R. L. Brutchey, *Chem. Sci.*, 2014, **5**, 2498–2502.
- P. D. Antunez, D. A. Torelli, F. Yang, F. A. Rabuffetti, N. S. Lewis and R. L. Brutchey, *Chem. Mater.*, 2014, **26**, 5444–5446.
- J. J. Buckley, M. J. Greaney and R. L. Brutchey, *Chem. Mater.*, 2014, **26**, 6311–6317.
- C. L. McCarthy, D. H. Webber, E. C. Schueller and R. L. Brutchey, *Angew. Chem. Int. Ed.*, 2015, **54**, 8378–8381.
- X. Zhao, M. Lu, M. J. Koeper and R. Agrawal, *J. Mater. Chem. A*, 2016, **4**, 7390–7397.
- Y. Yang, G. Wang, W. Zhao, Q. Tian, L. Huang and D. Pan, *ACS Appl. Mater. Interfaces*, 2015, **7**, 460–464.
- C. L. McCarthy and R. L. Brutchey, *Chem. Commun.*, 2017, **53**, 4888–4902.
- C. L. McCarthy, P. Cottingham, K. Abuyen, E. C. Schueller, S. P. Culver and R. L. Brutchey, *J. Mater. Chem. C*, 2016, **4**, 6230–6233.
- C. L. McCarthy and R. L. Brutchey, *Chem. Mater.*, 2017, **30**, 304–308.
- H. Zhou, F. Yu, Y. Liu, J. Sun, Z. Zhu, R. He, J. Bao, W. A. Goddard, S. Chen and Z. Ren, *Energy Environ. Sci.*, 2017, **10**, 1487–1492.
- I. H. Kwak, H. S. Im, D. M. Jang, Y. W. Kim, K. Park, Y. R. Lim, E. H. Cha and J. Park, *ACS Appl. Mater. Interfaces*, 2016, **8**, 5327–5334.
- M. Zeng and Y. Li, *J. Mater. Chem. A*, 2015, **3**, 14942–14962.
- M. S. Faber, M. A. Lukowski, Q. Ding, N. S. Kaiser and S. Jin, *J. Phys. Chem. C*, 2014, **118**, 21347–21356.
- F. Liu, J. Zhu, L. Hu, B. Zhang, J. Yao, M. K. Nazeeruddin, M. Grätzel and S. Dai, *J. Mater. Chem. A*, 2015, **3**, 6315–6323.
- X. Zhao, J. Jiang, Z. Xue, C. Yan and T. Mu, *Chem. Commun.*, 2017, **53**, 9418–9421.
- C. L. McCarthy, C. A. Downes, E. C. Schueller, K. Abuyen and R. L. Brutchey, *ACS Energy Lett.*, 2016, **1**, 607–611.
- F. Liu, J. Zhu, Y. Li, J. Wei, M. Lv, Y. Xu, L. Zhou, L. Hu and S. Dai, *J. Power Sources*, 2015, **292**, 7–14.
- C. L. McCarthy, C. A. Downes and R. L. Brutchey, *Inorg. Chem.*, 2017, **56**, 10143–10146.
- D. Voiry, H. S. Shin, K. P. Loh and M. Chhowalla, *Nat. Rev. Chem.*, 2018, **2**, 0105.
- C. C. L. McCrory, S. Jung, I. M. Ferrer, S. M. Chatman, J. C. Peters and T. F. Jaramillo, *J. Am. Chem. Soc.*, 2015, **137**, 4347–4357.
- X. Sun, Z. Xue and T. Mu, *Green Chem.*, 2014, **16**, 2102–2106.
- X. Sun, Y. Chi and T. Mu, *Green Chem.*, 2014, **16**, 2736–2744.
- N. Kornienko, J. Resasco, N. Becknell, C.-M. Jiang, Y.-S. Liu, K. Nie, X. Sun, J. Guo, S. R. Leone and P. Yang, *J. Am. Chem. Soc.*, 2015, **137**, 7448–7455.
- C. Zhang, C. P. Berlinguette and S. Trudel, *Chem. Commun.*, 2016, **52**, 1513–1516.
- J. Hu, C. Zhang, X. Meng, H. Lin, C. Hu, X. Long and S. Yang, *J. Mater. Chem. A*, 2017, **5**, 5995–6012.
- N. Suen, S. Hung, Q. Quan, N. Zhang, Y. Xu and H. M. Chen, *Chem. Soc. Rev.*, 2017, **46**, 337–365.
- R. Zhang, S. M. Szczepaniak, N. J. Carter, C. A. Handwerker and R. Agrawal, *Chem. Mater.*, 2015, **27**, 2114–2120.

Thiol – Amine Solution Processed Electrocatalysts



A thiol-amine solvent mixture was successfully utilized for the dissolution of bulk materials toward the solution deposition of chalcogenide electrocatalysts.